

Sleptons without Hadrons

Benjamin Fuks^{a,1,2}, Karl Nordström^{b,1,3}, Richard Ruiz^{c,4}, Sophie L. Williamson^{d,1}

¹ Laboratoire de Physique Théorique et Hautes Energies (LPTHE), UMR 7589, Sorbonne Université et CNRS, 4 place Jussieu, 75252 Paris Cedex 05, France

² Institut Universitaire de France, 103 boulevard Saint-Michel, 75005 Paris, France

³ National Institute for Subatomic Physics (NIKHEF) Science Park 105, 1098 XG Amsterdam, Netherlands

⁴ Centre for Cosmology, Particle Physics and Phenomenology (CP3),

Université Catholique de Louvain, Chemin du Cyclotron, 1348 Louvain la Neuve, Belgium

Received: date / Accepted: date

Abstract Multilepton searches for electroweakino and slepton pair production at hadron colliders remain some of the best means to test weak-scale supersymmetry. Searches at the CERN Large Hadron Collider, however, are limited by large diboson and top quark pair backgrounds, despite the application of traditional, central jet vetoes. In this context, we report the impact of introducing dynamic jet vetoes in searches for colorless superpartners. As a representative scenario, we consider the Drell-Yan production of a pair of right-handed smuons decaying into a dimuon system accompanied with missing transverse energy. As an exploratory step, we consider several global and local measures of the leptonic and hadronic activity to construct the veto. In almost all cases, we find that employing a dynamic jet veto improves the sensitivity, independently of the integrated luminosity. Directions for further improvements are discussed.

1 Introduction

Weak-scale supersymmetry, if realized in nature, presents an attractive solution to several longstanding theoretical and observational shortcomings of the Standard Model of particle physics (SM). For example, supersymmetry can protect the Higgs boson mass from large quantum corrections, ensure gauge coupling unification at high scales, and provide a viable weakly interacting dark matter candidate [1, 2]. While light, sub-TeV superpartners of quarks and gluons have largely been excluded by direct searches at the CERN Large Hadron Collider (LHC) [3–6], the situation is far less conclusive for electroweak (EW) boson and lepton superpartners due to their smaller production cross sections [7, 8].

^afuks@lpthe.jussieu.fr

^bknordstrom@lpthe.jussieu.fr

^crichard.ruiz@uclouvain.be

^dswilliamson@lpthe.jussieu.fr

Current constraints only exclude slepton masses up to a few hundreds of GeV [9, 10]. For electroweak boson partners [11–13], the case is slightly more interesting due to several small excesses, which reveal a local significance of 3.5σ and favor 100 – 300 GeV neutralino and chargino masses in the Minimal Supersymmetric Standard Model (MSSM) [14]. Hence, studies into new analysis strategies that can improve searches for electroweakinos and sleptons are highly motivated.

Among the several promising lines of such investigations are those that consider the impact of jet vetoes (*i.e.*, the rejection of events featuring jets with a transverse momentum greater than some threshold p_T^{Veto} [15–19]) in measurements of and searches for heavy, colorless SM [20–32] and beyond the SM [33–39] states. Interestingly, recent studies of multilepton searches for colorless exotic particles have demonstrated that dynamic jet vetoes can significantly improve their discovery potential [38, 39]. More specifically, a proposed analysis premised on setting p_T^{Veto} on an event-by-event basis to the hardness (p_T) of the event’s leading lepton was found to improve sensitivity by roughly an order of magnitude [38]. While serving a similar goal, such a veto functions in a qualitatively different manner than rapidity-dependent vetoes [26, 28, 29] by associating p_T^{Veto} with a measure of the hard process scale Q . A key point is that the improvement, which was demonstrated for both the Drell-Yan (DY) and electroweak boson fusion processes, followed from the veto largely acting to discriminate local leptonic activity from global hadronic activity [39].

In light of this, we have explored the impact of dynamic jet vetoes on the discovery potential of dimuon plus missing energy searches for right-handed smuon pairs ($\tilde{\mu}_R^+ \tilde{\mu}_R^-$) decaying to neutralinos ($\tilde{\chi}_1$) via the DY mode,

$$q\bar{q} \rightarrow \gamma^*/Z^{(*)} \rightarrow \tilde{\mu}_R^+ \tilde{\mu}_R^- \rightarrow \mu^+ \mu^- \tilde{\chi}_1 \tilde{\chi}_1, \quad (1)$$

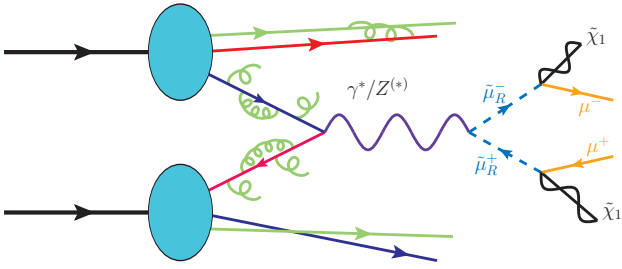


Fig. 1 Drell-Yan production of a pair of right-handed smuons ($\tilde{\mu}_R^+ \tilde{\mu}_R^-$) decaying into a pair of muons (μ^\pm) and lightest neutralinos ($\tilde{\chi}_1$). Generated with JAXODRAW [40].

as illustrated in fig. 1. We consider several measures of local and global leptonic and hadronic activity, including the scalar sum of the lepton transverse momenta (S_T) as well as the (inclusive) scalar sum of the transverse momenta of all hadronic objects (H_T), and focus on a benchmark CMS-inspired analysis [9] that features a standard (flavor-independent), static, central jet veto of $p_T^{\text{veto}} = 25$ GeV. As will be shown below, a dynamic veto can improve the discovery potential of the analysis in most cases.

The remainder of this report continues in the following manner: in sec. 2, we introduce our simplified model describing right-handed smuon production and decay in hadron collisions, and discuss the present constraints on the model. In sec. 3, we summarize our computational setup, which includes state-of-the-art event generation up to next-to-leading order (NLO) in QCD matched to parton showers (PS). We discuss slepton pair production at the LHC and the qualitative impact of different dynamic jet vetoes for the signal and background processes in sec. 4. There we also define our proposed dynamic veto and benchmark collider analyses. In sec. 5 we present our results and outlook, before summarizing and concluding in sec. 6.

2 Model

In order to investigate smuon production in a model-independent way, we focus on a benchmark simplified model inspired by the MSSM. We consider an MSSM limit in which all superpartners are decoupled, with the exception of the right-handed smuon $\tilde{\mu}_R$ (of mass $m_{\tilde{\mu}_R}$) and the lightest neutralino $\tilde{\chi}_1$ (of mass $m_{\tilde{\chi}_1}$) that is taken as bino-like. The Lagrangian describing the new physics dynamics of our model is given, using four-component fermion notations, by

$$\begin{aligned} \mathcal{L} = & [\partial_\mu \tilde{\mu}_R^\dagger] [\partial^\mu \tilde{\mu}_R] + \frac{i}{2} \bar{\tilde{\chi}}_1 \not{\partial} \tilde{\chi}_1 - m_{\tilde{\mu}_R}^2 \tilde{\mu}_R^\dagger \tilde{\mu}_R - \frac{1}{2} m_{\tilde{\chi}_1} \bar{\tilde{\chi}}_1 \tilde{\chi}_1 \\ & + \left[\partial^\mu \tilde{\mu}_R^\dagger \tilde{\mu}_R - \tilde{\mu}_R^\dagger \partial^\mu \tilde{\mu}_R \right] \left[ieA_\mu - \frac{ies_W}{c_W} Z_\mu \right] \\ & - \frac{\sqrt{2}e}{c_W} \left[\left(\bar{\tilde{\chi}}_1 P_R \mu \right) \tilde{\mu}_R^\dagger + \text{H.c.} \right] \end{aligned} \quad (2)$$

Here, we have explicitly indicated the smuon gauge interactions with the photon A_μ and Z boson field Z_μ (second line), as well as the supersymmetric gauge interactions of the muon μ , the smuon $\tilde{\mu}_R$, and the bino $\tilde{\chi}_1$ (last line). As irrelevant for our purposes, D -term contributions are neglected. In our notation, s_W and c_W are the sine and cosine of the electroweak mixing angle, e is the electromagnetic coupling constant, and P_R the right-handed chirality projector.

Despite its simplicity, the model is only weakly constrained by LHC searches for smuon pair production in the dimuon plus missing transverse energy channel [9]. This is due to large backgrounds, consisting mainly of W boson and top quark pair production, as well as being an electroweak signal production mode, as illustrated by eq. (1). For a massless neutralino, the smuon mass is constrained with $\mathcal{L} = 39.5 \text{ fb}^{-1}$ of $\sqrt{s} = 13$ TeV data to satisfy, at the 95% confidence level (CL), $m_{\tilde{\mu}_R} > 220$ GeV. There is almost no constraint when the neutralino is heavier than 100 GeV.

As the neutralino is stable, it is a viable candidate for a dark matter particle. Bino dark matter with light sleptons can be accommodated provided that the slepton-neutralino mass splitting is of at most 10% of the neutralino mass. Under this condition, there is sufficient co-annihilations so that the universe is not overclosed [41]. However, in the aim of using simplified models as tools for characterizing given phenomena, this latter constraint is ignored.

3 Computational Setup

To conduct our study, we simulate and analyze signal and background events in pp collisions at a center-of-mass energy $\sqrt{s} = 14$ TeV. We implement the simplified model Lagrangian of eq. (2) into FEYNRULES [42], that we jointly use with the NLOCT [43] and FEYNARTS [44] packages to generate a UFO library [45] that includes tree-level vertices as well as ultraviolet and R_2 counterterms (which enables numerical computations up to one-loop in the strong coupling constant α_s). Event generation for signal and background processes is performed with MADGRAPH5_AMC@NLO v2.6.3.2 [46], allowing us to match NLO QCD fixed-order calculations with parton showers with the MC@NLO prescription [47]. We use the MADSPIN [48] and MADWIDTH [49] programs to handle the smuon decays into a muon-neutralino system, and we rely on PYTHIA v8.230 [50], steered by the CUETP8M1 ‘‘Monash’’ tune [51], to handle parton showering (including QED effects), the hadronization of all final-state partons, as well as the decays of hadrons and tau leptons. Particle-level reconstruction is handled with MADANALYSIS5 v1.7.10 [52, 53], in which we enforce jet clustering following the anti- k_T algorithm [54], as implemented in FAST-

JET v3.3.0 [55]. We choose a jet radius of $R = 1$, following the jet veto analysis of ref. [37]. During the clustering procedure, ideal b -jet, light-jet, and hadronic tau (τ_h) tagging is assumed; potential misidentification of one particle species as another is implemented at the analysis level. Computations use the NNPDF 3.1 NLO+LUXQED parton distribution function (PDF) set [56], while both PDF and $\alpha_s(\mu)$ evolutions are managed by using LHAPDF 6 v1.7 [57].

In addition to event generation, totally inclusive cross section normalizations at NLO and with next-to-leading logarithmic (NLL) threshold corrections are obtained with RESUMMINO v2.0.1 [58]. We use again the NNPDF 3.1 NLO+LUXQED PDF set, despite the availability of PDFs extracted using threshold-corrected matrix elements [59]. Our choice is motivated by the much larger statistical uncertainty associated with the resummed PDF, which obfuscates their improved perturbative precision / systematic uncertainty. We refer to ref. [60] for a study of their impact on the hadroproduction of slepton pairs.

For total signal rates up to NLO+NLL, the collinear factorization (μ_f) and QCD renormalization (μ_r) scales are set to the smuon mass. For signal and background event generation, we use an event-by-event scale set to half the scalar sum of the transverse energy of all final-state particles,

$$\mu_{f,r} = \xi \times \mu_0 \quad \text{with} \quad \mu_0 = \frac{1}{2} \sum_{k \in \{\text{final state}\}} \sqrt{|p_T^k|^2 + m_k^2}. \quad (3)$$

By default, we set $\xi = 1$. The residual perturbative scale dependency is then quantified by varying μ_r and μ_f independently over the discrete range $\xi \in \{0.5, 1.0, 2.0\}$.

4 Smuon Pairs at the LHC

4.1 Smuon Pair Production

Like electroweakinos, sleptons can be produced through a variety of mechanisms in proton-proton collisions. For simplicity, we restrict ourselves to right-handed smuon pair production through the inclusive, Drell-Yan process,

$$pp \rightarrow \gamma^*/Z^* + X \rightarrow \tilde{\mu}_R^+ \tilde{\mu}_R^- + X, \quad (4)$$

as illustrated in fig. 1. At the hadronic level, X here denotes an arbitrary number of (predominantly forward) QCD jets. If vector boson fusion becomes a relevant production mode of TeV-scale smuons [61–63], as for example at higher collider energies and integrated luminosities beyond the LHC, then one can expect much of the same dynamic jet veto behavior as presented below [39].

In the upper panel of fig. 2, we show the totally inclusive NLO+NLL cross section for neutral-current DY smuon production at a center-of-mass energy $\sqrt{s} = 14$ TeV. The results are given as a function of the smuon mass, and we indicate

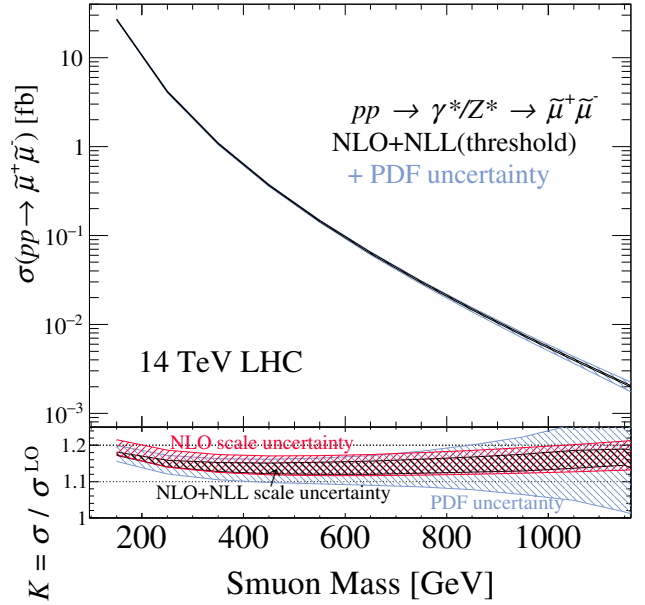


Fig. 2 Upper: totally inclusive neutral-current DY production cross section of $\tilde{\mu}_R^+ \tilde{\mu}_R^-$ pairs at NLO+NLL, and at a center-of-mass energy $\sqrt{s} = 14$ TeV with scale uncertainty (black band) and PDF uncertainty (lightest band). Lower: NLO+NLL (black band) and NLO (lighter band) QCD K -factor, with PDF uncertainty (lightest band).

the uncertainties stemming from perturbative scale variation (black band) and PDF fitting (light band). In the lower panel of the figure, we present QCD K -factors, with their uncertainties, defined relative to the Born process,

$$K^{\text{NLO+N}^k\text{LL}} = \frac{\sigma^{\text{NLO+N}^k\text{LL}}(pp \rightarrow \tilde{\mu}_R^+ \tilde{\mu}_R^- + X)}{\sigma^{\text{LO}}(pp \rightarrow \tilde{\mu}_R^+ \tilde{\mu}_R^- + X)}. \quad (5)$$

The cases $k = 0$ and $k = 1$, respectively, correspond to computations at NLO and NLO+NLL.

For smuon masses $m_{\tilde{\mu}_R} \in [200, 900]$ GeV (*i.e.*, the range of interest for the LHC), the NLO+NLL production cross section varies from approximately 10 fb to 10 ab, with the corresponding scale uncertainties reaching the $\pm 2 - 3\%$ level. In this mass regime, NLO+NLL predictions sit well within the NLO perturbative uncertainty band that has a width of about $\pm 4\%$. Furthermore, the QCD K -factors for both the NLO and NLO+NLL computations are of about $K \approx 1.15$ and largely independently of the smuon mass. On different grounds and still in this mass range, PDF uncertainties are only marginally larger than the NLO scale uncertainties, before growing significantly for $m_{\tilde{\mu}_R} \gtrsim 800$ GeV (due to the absence of data in the PDF fits). As the same PDF set is used for both the NLO and NLO+NLL computations, the size of their uncertainties is essentially identical.

For the parameter space consistent with our simplified model assumptions, the gluon fusion contribution to inclusive $\tilde{\mu}_R^+ \tilde{\mu}_R^-$ production, which formally arises at $\mathcal{O}(\alpha_s^2)$, is small compared with the neutral-current DY component [64, 65]. Moreover, for TeV-scale DY-like processes, QCD scale

uncertainties in cross sections featuring a dynamic jet veto at NLO+PS (which are formally at the leading-logarithmic accuracy) are comparable with the total inclusive cross section uncertainty at NLO due to the absence of large jet veto logarithms [38, 39]. This holds independently of the jet radius for a dynamic veto [39]. For a static veto, choosing a jet radius of $R = 1$ significantly helps to minimize the perturbative uncertainties [37, 66–68], though worsens the universal non-perturbative ones [27, 37, 69]. Thus, we may conclude that the cross section for $\tilde{\mu}_R^+ \tilde{\mu}_R^-$ production, either with or without a dynamic jet veto, as obtained from event generation at NLO+PS is an excellent estimate of the true rate. For our purposes and for discovery purposes, NNLO and NNLL (threshold) terms in fixed order and resummed signal predictions can be ignored.

4.2 Dynamic Jet Vetoes Beyond p_T

Jet vetoes have long been established as powerful tools to improve the discovery potential of sleptons and electroweakinos in multilepton searches at hadron colliders [33–35, 70]. In practice, LHC experiments rely on fixed/static veto thresholds of $p_T^{\text{veto}} = 20 - 50$ GeV for central jets within a pseudorapidity $|\eta^j| \lesssim 2.5$ [10, 71–76]. Recently [38, 39], though, it was demonstrated that dynamic jet veto schemes, namely ones wherein p_T^{veto} is set on an event-by-event basis to the p_T of an event’s leading lepton, can improve the sensitivity of multilepton searches for exotic, colorless particles. In conjunction with selection cuts on leptonic observables, this type of jet veto ultimately discriminates against the relative amounts of hadronic and leptonic activity in each event.

In this sense, dynamic jet vetoes can be generalized by considering observables that measure an event’s global hadronic and leptonic activities instead of just the p_T of an event’s leading objects. The inclusive scalar sum of p_T of all hadrons in an event ($H_T^{\text{Incl.}}$),

$$H_T^{\text{Incl.}} = \sum_{k \in \{\text{hadrons}\}} |\mathbf{p}_T^k| \approx \sum_{k' \in \{\text{jets}\}} |\mathbf{p}_T^{k'}|, \quad |\eta^{k,k'}| \lesssim 4.5, \quad (6)$$

or the exclusive scalar sum of p_T of the two leading charged leptons (ℓ_1, ℓ_2) in an event ($S_T^{\text{Excl.}}$),

$$S_T^{\text{Excl.}} = \sum_{k=1}^2 |\mathbf{p}_T^{\ell_k}|, \quad (7)$$

for example, are natural candidates. Here we adopt the usual particle ordering for leptons and jets, where $p_T^{k_i} > p_T^{k_{i+1}}$ for particles k_i and k_{i+1} of particle species k . We also henceforth suppress the “Incl./Excl.” labels for brevity but stress that we do not expect results here to uniformly carry over to exclusive H_T and inclusive S_T .

Qualitatively, H_T differs from the p_T of the leading (or subleading) central jet $p_T^{j_1}$ (or $p_T^{j_2}$) in that H_T is much more sensitive to complicated color topologies in a hard scattering processes. The simplest color topologies, *e.g.*, eq. 4, have at most one or two color dipoles / antennas, and hence less QCD radiation, resulting in H_T that is comparable to $p_T^{j_1}$. On the other hand, complex QCD processes, *e.g.*, $pp \rightarrow WW + nj$, have many color antennas, and hence more sources of QCD radiation, resulting in H_T significantly larger than $p_T^{j_1}$. Metaphorically speaking, H_T vs. $p_T^{j_1}$ is like a multi-band vs. single-band radio receiver, with complex color structures inducing many bands of radiation simultaneously whereas signal-like topologies have fewer bands.

Due to its exclusive nature, S_T acts to exaggerate and accentuate the characteristic behavior of the leading charged leptons ℓ_1 and ℓ_2 . If they stem from a resonant (continuum) process, then S_T will characteristically have a narrow (shallow) distribution. If the two are pair-produced, then one expects the scaling $S_T \sim 2p_T^{\ell_1}$. Likewise, any relative (in)dependence of $p_T^{\ell_k}$ on the hadronic activity is inherited by S_T . By virtue of the Collinear Factorization Theorem, central, high- p_T charged leptons in hadron collisions stem from a hard underlying process. Hence, the S_T of leading leptons probes an event’s hard-scattering core, and must scale like the hard scattering scale Q . This helps to protect against the emergence of large veto logarithms. Exclusive S_T differs from inclusive S_T in that the latter sums over the trailing charged leptons and additionally probes universal, low- Q^2 physics, such as hadron decays and QED parton showering.

In application, a dynamic, H_T -based jet veto would work, for example, by rejecting events in which H_T exceeds $p_T^{\ell_1}$. Analogously, an S_T -based veto functions by requiring, for example, an event to satisfy $p_T^{j_1} < S_T$ for $|\eta^{j_1}| < \eta^{\text{max}}$.

To explore these alternative dynamic veto schemes, we present in fig. 3, the normalized distributions for the following ratios of leptonic and hadronic activities:

$$\begin{aligned} \text{(a)} & p_T^{\ell_1}/p_T^{j_1}, & \text{(b)} & p_T^{\ell_1}/H_T, & \text{(c)} & S_T/p_T^{j_1}, \\ \text{(d)} & S_T/H_T, & \text{(e)} & p_T^{\ell_2}/p_T^{j_1}, & \text{(f)} & p_T^{\ell_2}/H_T. \end{aligned}$$

These are considered for the signal process given in eq. 4, assuming three benchmark parameter space points,

$$\begin{aligned} \text{Signal Category : } & (m_{\tilde{\mu}_R}, m_{\tilde{\chi}_1}), \\ \text{High-mass, Large mass splitting : } & (750 \text{ GeV}, 100 \text{ GeV}), \\ \text{High-mass, Small mass splitting : } & (750 \text{ GeV}, 700 \text{ GeV}), \\ \text{Low-mass, Small mass splitting : } & (100 \text{ GeV}, 50 \text{ GeV}), \end{aligned}$$

with smuons decaying into an SM muon and a neutralino. We also consider the representative backgrounds,

$$pp \rightarrow t\bar{t} \rightarrow \ell^+ \ell^- + X, \quad pp \rightarrow \ell^+ \ell^- \nu\bar{\nu}, \quad (8)$$

with $\ell \in \{e, \mu, \tau_h\}$. All signal and background processes are considered at NLO+PS, after jet clustering. We require at

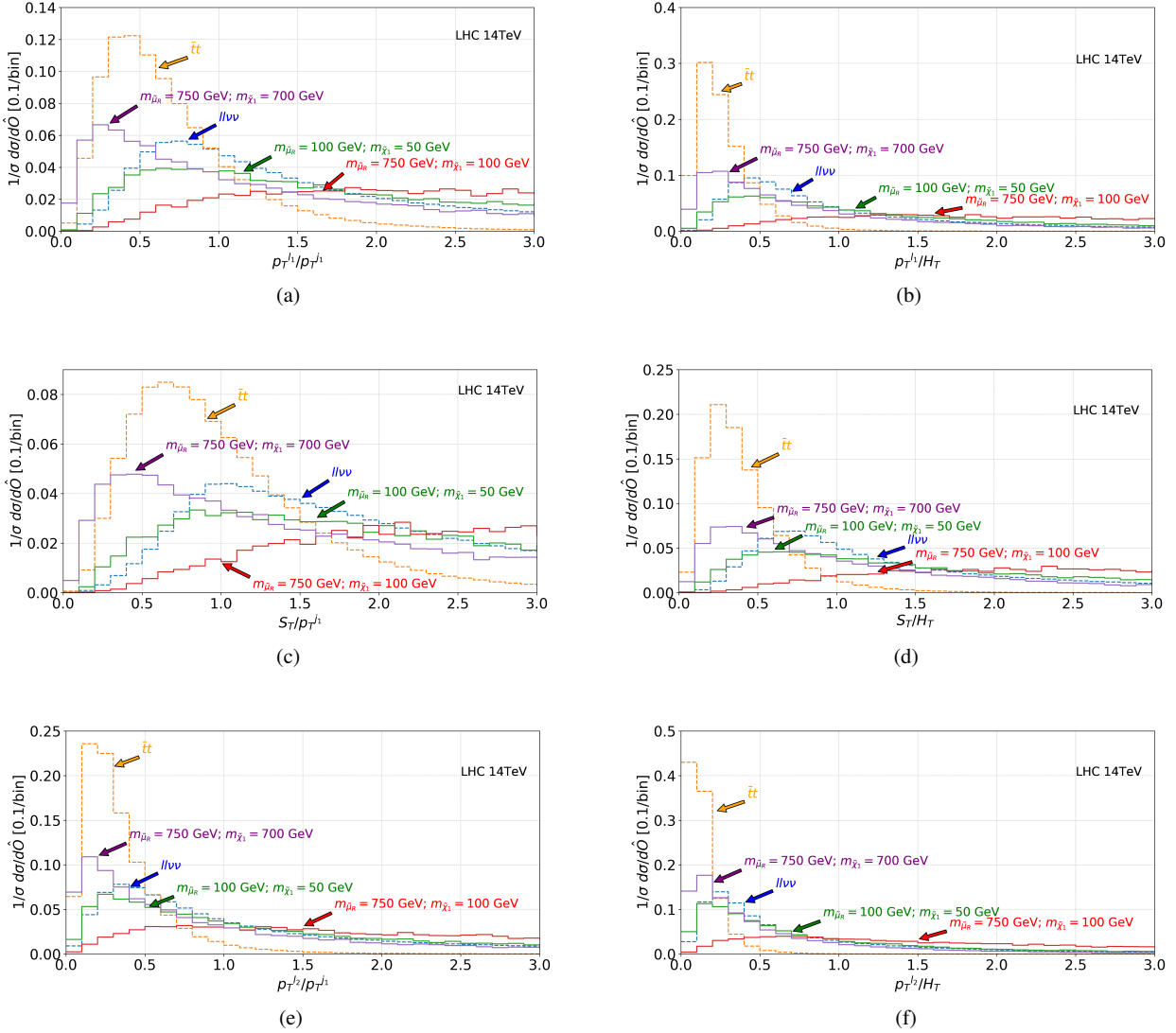


Fig. 3 Ratios of measures of hadronic and leptonic activity for representative signal (solid) and background (dashed) samples used in the dynamic veto analysis, showing (a) $p_T^{\ell_1}/p_T^{j_1}$, (b) $p_T^{\ell_1}/H_T$, (c) $S_T/p_T^{j_1}$, (d) S_T/H_T , (e) $p_T^{\ell_2}/p_T^{j_1}$, (f) $p_T^{\ell_2}/H_T$.

least two oppositely charged muons with any number of jets satisfying the nominal truth-level kinematical requirements

$$|\eta^\ell| < 2.4 \quad \text{and} \quad p_T^\ell > 10 \text{ GeV}. \quad (9)$$

As a reference point, we discuss first the kinematic ratio $r_{j_1}^{\ell_1} = p_T^{\ell_1}/p_T^{j_1}$, as studied by refs. [38, 39] and shown in fig. 3(a). For the signal processes, we see a difference in behavior according to whether or not the smuon and neutralino are close in mass. Whereas the high-mass, large mass splitting configuration possesses a very broad distribution, with most of the phase space exceeding $r_{j_1}^{\ell_1} > 1$, the more compressed configurations possess relatively narrower distributions, with significantly more phase space below the $r_{j_1}^{\ell_1} = 1$ threshold. For the large

mass splitting case, final-state muons carry $p_T^\ell \sim m_{\tilde{\mu}_R}(1 - m_{\tilde{\chi}_1}^2/m_{\tilde{\mu}_R}^2)/2 \sim m_{\tilde{\mu}_R}/2 \sim 375 \text{ GeV}$. This is significantly larger than the leading jet p_T , which is generally of the order of the Sudakov peak. For on-shell slepton pair production, the Sudakov peak is much lower than $2m_{\tilde{\mu}_R}$, indicating that characteristically $p_T^{j_1} \ll p_T^{\ell_1} \sim m_{\tilde{\mu}_R}/2$. For the compressed cases, the muons carry only $p_T^\ell \lesssim 40 - 50 \text{ GeV}$ and drive the relationship $r_{j_1}^{\ell_1}$ (high-mass, small-splitting.) $\lesssim r_{j_1}^{\ell_1}$ (low-mass, small-splitting.) $\lesssim 1$.

Considering the background processes, one observes that most events populate the region around $r_{j_1}^{\ell_1} \sim 0.25 - 0.75$. In both cases, the behavior follows from kinematic arguments [38]. For an at-rest top quark decaying into leptons, the characteristic momenta of the charged lepton and asso-

ciated b -quark give rise to the scaling

$$r_{j_1}^{\ell_1} \sim \frac{p_T^\ell}{p_T^b} \sim \frac{m_t (1 + M_W^2/m_t^2)/4}{m_t (1 - M_W^2/m_t^2)/2} \sim 0.75. \quad (10)$$

In a full simulation at NLO+PS with large- R jets, this is pushed significantly to smaller values due to a large $t\bar{t} + 1j$ sub-channel, boosts from large ($t\bar{t}$)-invariant masses, and into-cone radiation. Each enhances p_T^j or p_T^b relatively to p_T^ℓ . Despite being a color-singlet process, the inclusive $pp \rightarrow \ell\ell\nu\nu + X$ channel has a relatively large $pp \rightarrow \ell\ell\nu\nu + 1j$ fraction. This is due to the Born-like $pp \rightarrow W\gamma^*/WZ + 0j$ processes being suppressed by radiation zeroes [77–84]. In turn, $r_{j_1}^{\ell_1}$ is inherently less than unity.

In fig. 3(b), we consider the impact of additional QCD radiation and show the distribution for $r_{H_T}^{\ell_1} = p_T^{\ell_1}/H_T$. For the signal processes, we observe some difference from $r_{j_1}^{\ell_1}$ in the normalization and position of the distributions' maxima. Here, the maxima are marginally taller and pushed to slightly lower values of $r_{H_T}^{\ell_1}$. This is indicative of the low hadronic activity in DY-like processes, which is in fact why a jet veto is considered at all. On the other hand, for both background processes, we observe values of $r_{H_T}^{\ell_1}$ much smaller than $r_{j_1}^{\ell_1}$. For $t\bar{t}$ specifically, the shift (and narrowing) from $r_{j_1}^{\ell_1} \lesssim 0.5$ to $r_{H_T}^{\ell_1} \lesssim 0.25$ is consistent with H_T , which sums over both bottom jets, being roughly $1/H_T \sim 1/(2 \times p_T^{j_1}) \sim 1/(2 \times p_T^{b_1})$. The low-mass, compressed signal distribution is in particular hardly distinguishable from the $\ell\ell\nu\nu$ distribution.

Considering now a more global measure of leptonic activity, we present in figs. 3(c) and (d) the distributions for the ratios $r_{j_1}^{S_T} = S_T/p_T^{j_1}$ and $r_{H_T}^{S_T} = S_T/H_T$, respectively. For all cases we see that the $r_{j_1}^{S_T}$ and $r_{H_T}^{S_T}$ curves are broader than their $r_{j_1}^{\ell_1}$ and $r_{j_1}^{S_T}$ counterparts, and that the distributions' maxima are shifted slightly rightward. As in the (a) and (b) panels, the compressed signals and both background processes have a significant fraction of the phase space below unity.

As an alternative measure of local leptonic activity, we show in fig. 3(e) and (f) the distributions for the ratios $r_{j_1}^{\ell_2} = p_T^{\ell_2}/p_T^{j_1}$ and $r_{H_T}^{\ell_2} = p_T^{\ell_2}/H_T$, respectively. Immediately, one sees a larger separation than in (a) and (c) of the high-mass, compressed signal process from all other processes. Notably, the $t\bar{t}$ distributions are much narrower, with almost all events falling below $r_{j_1}^{\ell_2} \lesssim 0.5$ and $r_{H_T}^{\ell_2} \lesssim 0.25$.

Taken together, a picture emerges for generalized definitions of dynamic jet vetoes. We find that all of the proposed veto schemes exhibit uniform behavior. For the signal process with the highest charged lepton momenta, *i.e.*, the high-mass, large mass splitting signal category, we find a clear signal-to-background separation against representative background processes. For signal processes with charged

lepton momenta comparable to SM processes, we find significantly less but nonetheless interesting discriminating power. In particular, for the low-mass, compressed category, we observe reasonable separation from $t\bar{t}$ but poor separation from $\ell\ell\nu\nu$, whereas for the high-mass, compressed category we report the opposite. This suggests that it may be possible to salvage additional signal space with complementary selection cuts. Quantitatively, we observe a larger signal-to-background separation for dynamic veto schemes with more inclusive/global hadronic observables, *e.g.*, H_T , and more exclusive/local charged lepton observables, *e.g.*, $p_T^{\ell_2}$. The worst separation is given by $r_{j_1}^{S_T}$, which makes use of the multilepton activity of background processes but not the relatively low hadronic activity of the signal processes. The ratio $r_{H_T}^{\ell_2}$ appears to be exceptionally powerful in rejecting top quark background.

4.3 Jet Veto Collider Analyses

We now turn to defining our static and dynamic jet veto analyses to quantify how generalized dynamic jet vetoes may improve the discovery potential of smuon pairs at the LHC, if at all. For all analyses, we define analysis-quality charged leptons and jets as those that satisfy the following kinematical, fiducial, and isolation requirements,

$$p_T^{e(\mu)[\tau_h]\{j\}} > 10 \text{ (10) [20] \{25\} GeV, \\ |\eta^{e(\mu)[\tau_h]\{j\}}| < 2.4, \quad \Delta R_{\ell_m, \ell_n} > 0.4, \quad \Delta R_{\ell j} > 0.4.$$

We use the electron and muon efficiencies as reported¹ in ref. [9] for leptons with $p_T \geq 20$ GeV, and those reported in ref. [85] for leptons with $p_T \in [10, 20]$ GeV. We tag the hadronic decays of τ leptons (τ_h) with $p_T \geq 20$ GeV using the efficiencies reported in ref. [86]. All objects are smeared with a Gaussian profile as done in ref. [39], using publicly available resolution parameterizations as reported by the ATLAS and CMS collaborations [87–90]. The magnitude of the transverse momentum imbalance vector (\cancel{E}_T) is defined with respect to all visible momenta within $|\eta| < 4.5$,

$$\cancel{E}_T = |\cancel{\mathbf{p}}_T|, \quad \cancel{\mathbf{p}}_T = - \sum_{k \in \{\text{visible}\}} \mathbf{p}_T^k. \quad (11)$$

We consider the following background processes:

$$pp \rightarrow llll, \quad pp \rightarrow \ell\ell\nu, \quad pp \rightarrow \ell\ell\nu\nu, \quad pp \rightarrow \ell^+\ell^-, \\ pp \rightarrow t\bar{t} \rightarrow 2\ell X, \quad pp \rightarrow t\bar{t}\ell\nu \rightarrow 3\ell X, \\ pp \rightarrow WW\ell\ell \rightarrow 2\ell X, \quad pp \rightarrow WWW \rightarrow 3\ell X,$$

at NLO+PS, as modeled by ref. [39].

¹<https://twiki.cern.ch/twiki/bin/view/CMSPublic/SUSMoriond20170bjectsEfficiency>

Analysis Object Criteria at $\sqrt{s} = 14$ TeV: $p_T^e(\mu) [\tau_h] \{j\} > 10$ (10) [20] {25} GeV, $ \eta^e(\mu) [\tau_h] \{j\} < 2.4$, anti- k_T w./ $R = 1$ $\Delta R_{\ell_m, \ell_n} > 0.4$, $\Delta R_{\ell j} > 0.4$
Common Analysis Requirements: $N(\mu^+) = 1$, $N(\mu^-) = 1$, $N(\ell) = 2$, $m_{\mu\mu} > 20$ GeV, $ m_{\mu\mu} - M_Z > 15$ GeV, $M_{T2} > 90$ GeV, $\cancel{E}_T > 100$ GeV, Binned signal region: $\cancel{E}_T \in$ (a)[100, 150[, (b)[150, 225[, (c)[225, 300[, (d)[300, ∞ [GeV
Benchmark (Static) Jet Veto Analysis Requirements: $p_T^{\mu_1(\mu_2)} > 50$ (20) GeV, $p_T^{\text{Veto}} = 25$ GeV
Dynamic Jet Veto Analysis Requirements: Overlapping Signal Categories: (a) $p_T^{\text{Veto}} = p_T^{\ell_1}$ (b) $H_T^{\text{Veto}} = p_T^{\ell_1}$ (c) $p_T^{\text{Veto}} = S_T$ (d) $H_T^{\text{Veto}} = S_T$ (e) $p_T^{\text{Veto}} = p_T^{\ell_2}$ (f) $H_T^{\text{Veto}} = p_T^{\ell_2}$

Table 1 (Top) Analysis object / particle identification requirements at $\sqrt{s} = 14$ TeV; (upper) common analysis requirements; (lower) benchmark static veto analysis requirements; and (bottom) dynamic jet veto analysis requirements.

Shared Analysis Baseline

As a baseline for all analyses, we follow closely the CMS search for slepton pair production in dilepton final states at $\sqrt{s} = 13$ TeV with $\mathcal{L} = 35.9 \text{ fb}^{-1}$ of data [9]. We pre-select events featuring one pair of analysis quality, opposite-sign muons, and veto events with additional analysis-quality charged leptons. We are thus inclusive with respect to additional leptons outside these criteria. Low-mass hadronic resonances and Z-pole contributions are removed with the invariant mass cuts: $m_{\mu\mu} > 20$ GeV and $|m_{\mu\mu} - M_Z| > 15$ GeV. The SM DY continuum is further suppressed by requiring $\cancel{E}_T > 100$ GeV, and diboson and top pair processes are reduced by requiring a “transverse mass” cut of $M_{T2} > 90$ GeV [91, 92]. In sec. 5, we describe the impact of relaxing this cut. Events are then binned according to \cancel{E}_T . Analysis object definitions and shared analysis requirements are summarized in the top two sections of table 1.

Benchmark, Static Jet Veto Analysis

At this point, our jet veto collider analyses diverge. Our benchmark, static jet veto analysis continues as prescribed in the baseline CMS analysis [9] and further requires that the p_T of the leading and subleading muons satisfy

$$p_T^{\ell_1(\ell_2)} > 50 \text{ (20) GeV.} \quad (12)$$

Lastly, we impose a static jet veto of $p_T^{\text{Veto}} = 25$ GeV on analysis-quality jets. As such objects must sit within $|\eta| <$

Cut	$\sigma(\ell\ell\nu\nu)$ [fb]	$\sigma(\ell\ell\nu)$ [fb]	$\sigma(t\bar{t})$ [fb]
Generator	11 000	2600	87 000
Dimuon Selection	820 (7.7%)	140 (5.5%)	6500 (7.4%)
+ $m_{\ell\ell}$ Requirements	560 (69%)	41 (28%)	5000 (78%)
+Minimum M_{T2}	2.9 (0.52%)	0.80 (2.0%)	7.8 (0.16%)
+ $p_T^{\ell_1} > 50$ GeV, $p_T^{\ell_2} > 20$ GeV	3.0 (96%)	0.76 (94%)	6.8 (96%)
+Static Jet Veto	1.5 (54%)	0.26 (35%)	0.034 (0.50%)
$\cancel{E}_T \in$ [100 – 150[GeV	0.80 (53%)	0.14 (53%)	0.017 (50%)
[150 – 225[GeV	0.35 (23%)	0.055 (21%)	0. (0.%)
[225 – 300[GeV	0.079 (5.3%)	0.012 (4.5%)	0. (0.%)
[300, ∞ [GeV	0.056 (3.8%)	0.0050 (2.0%)	0. (0.%)

Table 2 For representative SM backgrounds, the cross section [fb] and cut efficiency [%] for the selection cuts presented in table 1 of the reference static jet veto analysis.

2.4, the veto is more specifically a static, central jet veto. Analysis requirements are summarized in the third section of table 1.

For background processes, we find comparable cross sections after selection cuts to those reported by CMS for all signal regions except the lowest \cancel{E}_T bin. There, we find our background rate is about 50% lower and is driven by a difference in the normalization of the “Flavor Symmetric” background, which is largely populated by the $t\bar{t}$ and diboson processes. We attribute the difference in this bin to our background normalizations being accurate only up to NLO+PS, and are therefore missing numerically large $\mathcal{O}(\alpha_s^2)$ contributions. This contrasts with the CMS normalization that is set by data. The cutflow for the dominant backgrounds are summarized in table 2.

Dynamic Jet Veto Analysis

The goal of this study is to see to what extent generalizations of dynamic jet vetoes can improve searches for multilepton final states over traditional, static, central jet vetoes. To do this, we propose a class of analyses that simplifies the static veto analysis of the preceding subsection. We execute this by removing the stringent high- p_T selection cuts on charged leptons given in eq. (12) and by setting the central jet veto threshold on an event-by-event basis. More precisely, events are vetoed either (i) if there exists an analysis-quality jet

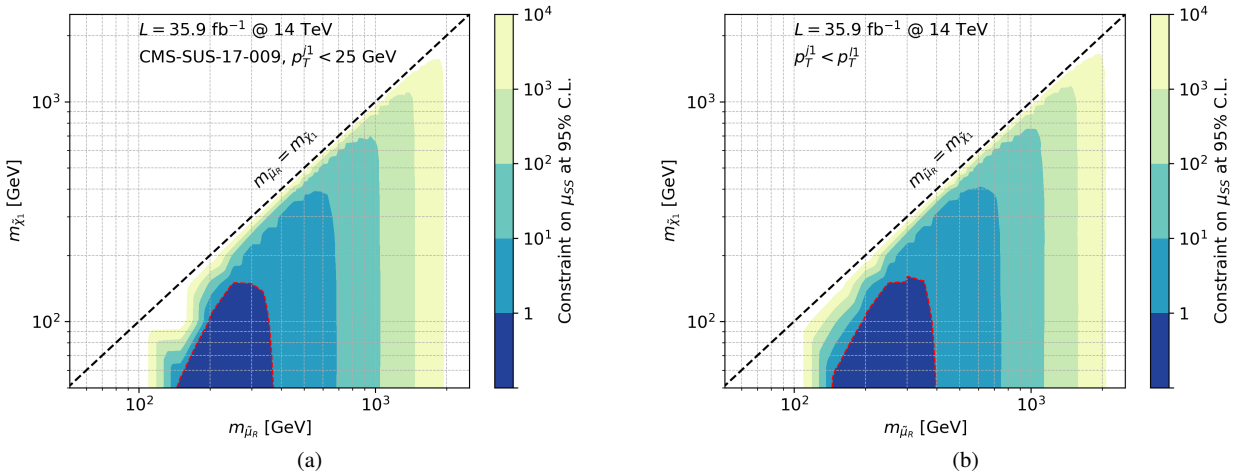


Fig. 4 Exclusion contours on the signal strength μ_{SS} for smuon pair production in the $(m_{\tilde{\chi}_1}, m_{\tilde{\mu}_R})$ plane with $\mathcal{L} = 35.9 \text{ fb}^{-1}$, for (a) the static jet veto analysis based on ref. [9], with $p_T^{\text{Veto}} = 25 \text{ GeV}$, and (b) the dynamic jet veto analysis with $p_T^{\text{Veto}} = p_T^{\ell_1}$.

with $p_T^j > p_T^{\text{Veto}}$ or (ii) if the event possess $H_T > H_T^{\text{Veto}}$. In no case do we consider simultaneously a veto on p_T^j and on H_T . The veto threshold are set dynamically according to the following permutations:

- (a) $p_T^{\text{Veto}} = p_T^{\ell_1}$, (b) $H_T^{\text{Veto}} = p_T^{\ell_1}$, (c) $p_T^{\text{Veto}} = S_T$,
 (d) $H_T^{\text{Veto}} = S_T$, (e) $p_T^{\text{Veto}} = p_T^{\ell_2}$, (f) $H_T^{\text{Veto}} = p_T^{\ell_2}$.

In principle, one can introduce a scaling factor r , e.g., $H_T^{\text{Veto}} = r \times S_T$, with $r = 0.75$, and improve the signal-to-background ratio S/B according to fig. 3. However, this is beyond the proof-of-concept scope of our study. Needless to say, investigations into optimizing a “smart jet veto” are encouraged.

5 Results and Outlook

To quantify the impact of dynamic jet vetoes on searches for smuon pairs, we use the CL_S technique [93] to first determine the 95% CL reach in terms of the event rate $N_{95} = \sigma_{95} \times \mathcal{L}$, for a luminosity \mathcal{L} . We take into account the Monte Carlo uncertainties for both the signal and the background, but do not consider additional systematic uncertainties. We use the combined likelihood ratio of the four signal regions as our test statistic. Sensitivity is then expressed in terms of the signal strength (μ_{SS}),

$$\mu_{SS} = \sigma_{95} / \sigma_p, \quad (13)$$

where σ_p is the predicted cross section in our simplified model. A signal strength of $\mu_{SS} < 1$ means that the signal hypothesis is excluded with at least 95% confidence.

As a check, we show in fig. 4, μ_{SS} for (a) the static jet veto analysis based on ref. [9], where $p_T^{\text{Veto}} = 25 \text{ GeV}$,

and (b) the dynamic jet veto $p_T^{\text{Veto}} = p_T^{\ell_1}$, assuming $\mathcal{L} = 35.9 \text{ fb}^{-1}$ at $\sqrt{s} = 14 \text{ TeV}$. We find that the constraints derived using the reference analysis are only slightly stronger than the reported in ref. [9]. This is attributed to three reasons. First, in comparison to the 13 TeV results explored with data, we take $\sqrt{s} = 14 \text{ TeV}$. Second, we do not consider additional systematic uncertainties, and finally, we recover a slightly smaller background prediction for the lowest \cancel{E}_T signal region compared with the data-driven prediction of ref. [9] (see sec. 4.3).

With the the dynamic jet veto analysis, we observe an improvement in sensitivity over the static veto analysis, with $m_{\tilde{\mu}_R} \lesssim 400 \text{ GeV}$ being accessible for $m_{\tilde{\mu}_R} \gg m_{\tilde{\chi}_1}$, to be confronted to $m_{\tilde{\mu}_R} \lesssim 375 \text{ GeV}$ in the static case. For $\mathcal{L} = 3000 \text{ fb}^{-1}$, we find that the improvement is very comparable. We stress that while the improvement appears limited due to the steeply falling signal cross section, it has been obtained by relaxing several selection cuts of the somewhat sophisticated analysis of ref. [9], and naively applying a dynamic jet veto that has not been optimized according to fig. 3. This “out-of-the-box” improvement even for relatively light smuon masses is encouraging.

To present our main results, for a given jet veto scheme and luminosity, we consider the ratio of signal strengths:

$$\mathcal{R}_{\text{Dy. Veto}} = \frac{\mu_{SS}^{\text{CMS}}}{\mu_{SS}^{\text{Dy. Veto}}} = \frac{\sigma_{95}^{\text{CMS}} / \sigma_p^{\text{CMS}}}{\sigma_{95}^{\text{Dy. Veto}} / \sigma_p^{\text{Dy. Veto}}}, \quad (14)$$

where μ_{SS}^{CMS} is the signal strength as determined using the reference static jet veto analysis and $\mu_{SS}^{\text{Dy. Veto}}$ is the signal strength as determined with the dynamic jet veto analysis. The double ratio has the simple interpretation that a value

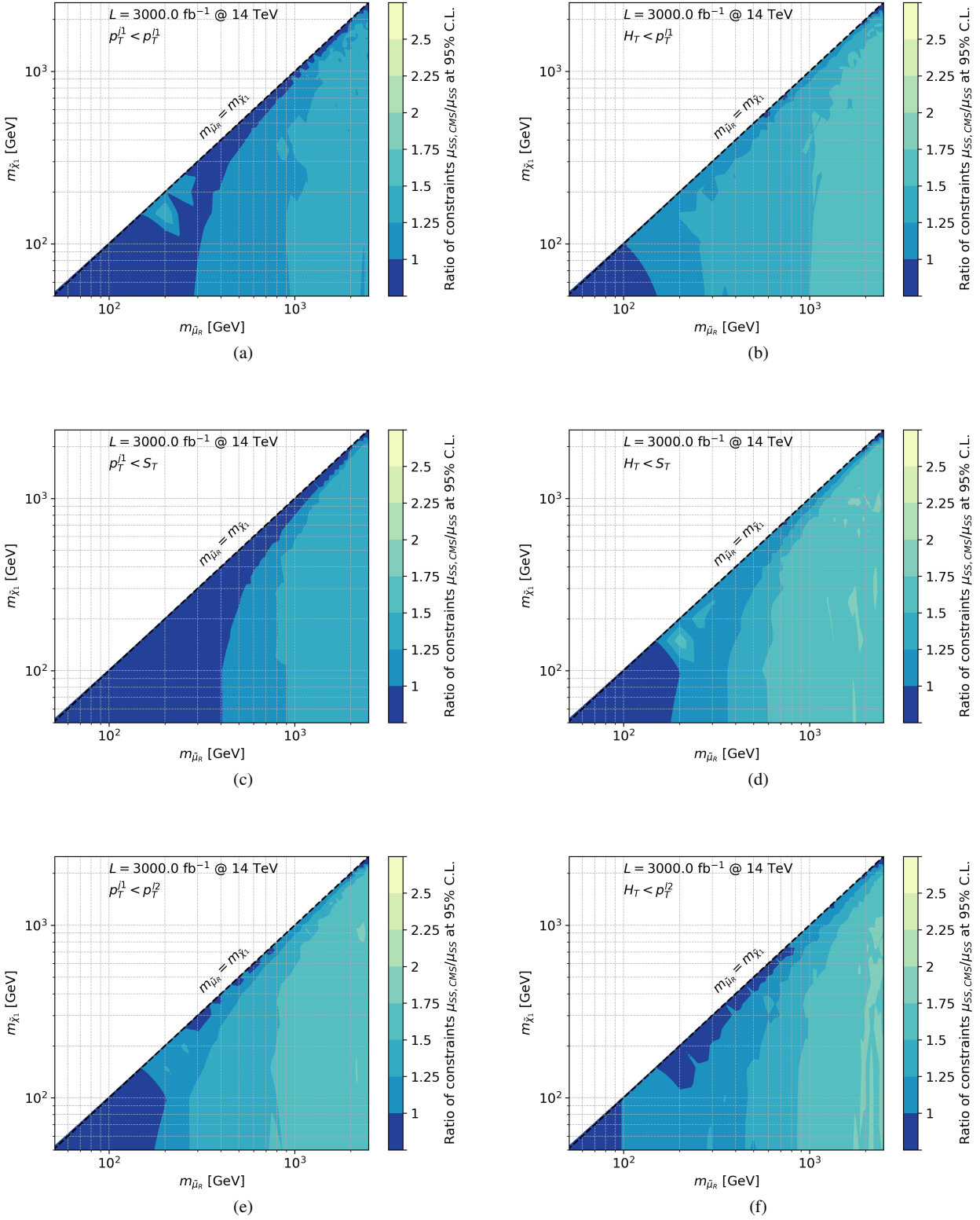


Fig. 5 The ratio of signal strengths (μ_{SS}) for (a) $p_T^{j1} < p_T^{l1}$, (b) $H_T < p_T^{j1}$, (c) $p_T^{j1} < S_T$, (d) $H_T < S_T$, (e) $p_T^{j1} < p_T^{l2}$, and (f) $H_T < p_T^{l2}$, compared with the CMS reference analysis using $\mathcal{L} = 3000 \text{ fb}^{-1}$.

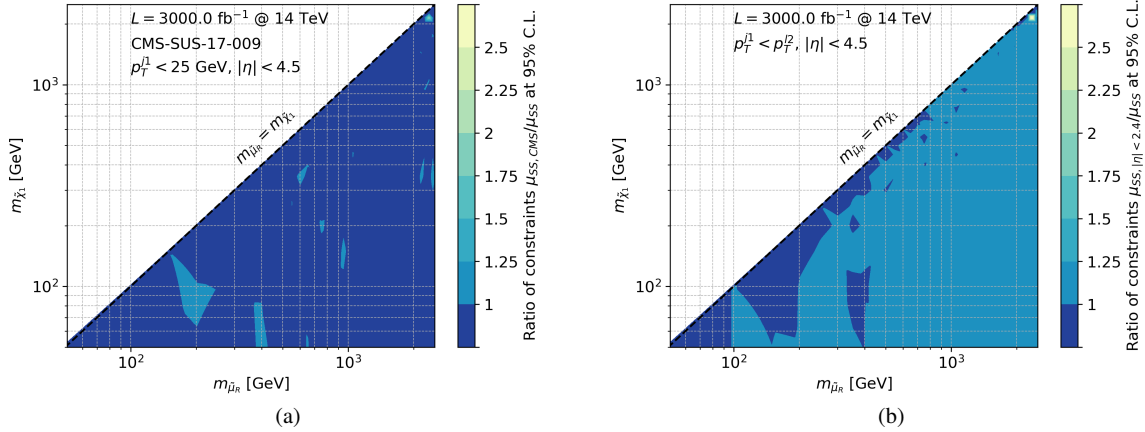


Fig. 6 The ratio of constraints at $\mathcal{L} = 3000 \text{ fb}^{-1}$ for (a) the default CMS analysis, and (b) the dynamic $p_T^{j1} < p_T^{j2}$, both with a jet pseudorapidity cut of $|\eta| < 4.5$, compared with their respective default analyses employing $|\eta| < 2.4$.

of $\mathcal{R} > 1$ implies that the dynamic veto analysis is more sensitive than the static veto analysis for a given input.

In fig. 5, assuming $\mathcal{L} = 3000 \text{ fb}^{-1}$, we present \mathcal{R} for

- (a) $p_T^{\text{Veto}} = p_T^{\ell_1}$, (b) $H_T^{\text{Veto}} = p_T^{\ell_1}$, (c) $p_T^{\text{Veto}} = S_T$,
 (d) $H_T^{\text{Veto}} = S_T$, (e) $p_T^{\text{Veto}} = p_T^{\ell_2}$, (f) $H_T^{\text{Veto}} = p_T^{\ell_2}$.

In the large mass splitting regime where $m_{\tilde{\mu}_R} \gg m_{\tilde{\chi}_1}$, we find that the veto scheme (f) $H_T^{\text{Veto}} = p_T^{\ell_2}$ outperforms the static veto analysis for $m_{\tilde{\mu}_R} \gtrsim 100 - 150 \text{ GeV}$; this finding extends to (b) $H_T^{\text{Veto}} = p_T^{\ell_1}$, (d) $H_T^{\text{Veto}} = S_T$ and (e) $p_T^{\text{Veto}} = p_T^{\ell_2}$ for $m_{\tilde{\mu}_R} \gtrsim 200 \text{ GeV}$; and we report that all dynamic jet veto schemes show improvement for $m_{\tilde{\mu}_R} \gtrsim 400 \text{ GeV}$. Of the schemes considered, the choice (c) $p_T^{\text{Veto}} = S_T$ performs worst, with the baseline static analysis outdoing the dynamic analysis for much of the phenomenologically relevant parameter space. Entertainingly, the dynamic veto (a) $p_T^{\text{Veto}} = p_T^{\ell_1}$ is one of the poorer veto schemes, relatively speaking, suggesting that the results of ref. [38, 39] can actually be further improved. For the compressed regime where $m_{\tilde{\mu}_R} \sim m_{\tilde{\chi}_1}$, the (b) $H_T^{\text{Veto}} = p_T^{\ell_1}$ and (d) $H_T^{\text{Veto}} = S_T$ schemes demonstrate uniform improvement, and partial improvement for (e) $p_T^{\text{Veto}} = p_T^{\ell_2}$ and (f) $H_T^{\text{Veto}} = p_T^{\ell_2}$.

For much of the parameter space of interest, we see that the improvement is in excess of 25 to 50%. The relative improvement grows with increasing $m_{\tilde{\mu}_R}$ since the static veto reduces the signal efficiency for heavier mass scales (due to harder initial-state radiation) while the dynamic veto schemes generally remain efficient or become more efficient (due to harder, final-state charged leptons). At lower $m_{\tilde{\mu}_R}$ and close to the degenerate limit, final-state leptons are relatively soft. This leads to p_T^{Veto} and H_T^{Veto} thresholds that are as tight as, if not more stringent than, the static veto, thereby eliminating any improvement from relaxing other selection cuts.

Qualitatively, we observe that H_T -based vetoes tend to perform better than p_T^{j1} -based vetoes, indicating the utility of veto schemes that employ more inclusive measures of the hadronic activity, *e.g.*, H_T . S_T -based schemes are competitive, in particular $H_T^{\text{Veto}} = S_T$ which is one of the strongest vetoes overall. On the other hand $p_T^{\text{Veto}} = S_T$ is too inclusive to be competitive except for large $m_{\tilde{\mu}_R}$. The inclusive nature of S_T is particularly useful in the compressed region for $H_T^{\text{Veto}} = S_T$, where individual lepton momenta are the smallest. In short, a whole class of dynamic jet vetoes can improve discovery potential of smuon pairs, but the difference in performance across the various limits of parameter space suggests that no single combination of hadronic and leptonic activity measures will be ideal in all cases. The appropriate leptonic measure should be investigated on an analysis-by-analysis basis in order to target specific kinematic regions.

Impact of Jet Veto Rapidity Window

Experimentally, jets can only be reconstructed within the range of the detector, *i.e.*, with a pseudorapidity $|\eta| \lesssim 4.5$ for ATLAS and CMS. In practice though, stringent, static jet vetoes are often only applied within the coverage of the tracker, typically for jets with $|\eta| \lesssim 2.4$. Extending jet vetoes to the forward region, $2.4 \lesssim |\eta| \lesssim 4.5$, is avoided, amongst other reasons, to help to mitigate the contamination of pile-up activity, including the contribution to low- p_T jets that would otherwise never exceed a veto threshold. This avoidance, however, is at the cost of an increased dependence on higher order QCD splittings, and hence an increased theoretical uncertainty [29]. On the other hand, it has recently been demonstrated that rapidity-dependent, jet vetoes, in particular one wherein p_T^{Veto} is relaxed for increasing jet pseudorapidity, can reduce this theoretical uncertainty [29], and are

already experimentally viable [94]. Moreover, extending dynamic jet vetoes to the forward region was found to be necessary to ensure a sufficient suppression of SM backgrounds in studies at higher \sqrt{s} [39].

In this context, we briefly investigate the impact of a dynamic jet veto when expanding the η range of the jet veto window from $|\eta| < 2.4$ to $|\eta| < 4.5$. For a widened η range, we show in fig. 6, the signal strength ratio,

$$\mathcal{R}_X = \mu_{SS}^X(|\eta^{\text{Veto}}| < 2.4) / \mu_{SS}^X(|\eta^{\text{Veto}}| < 4.5), \quad (15)$$

for (a) the benchmark static jet veto analysis, where $p_T^{\text{Veto}} = 25$ GeV, and (b) the dynamic analysis, with $p_T^{\text{Veto}} = p_T^{\prime 2}$. As before, a ratio of $\mathcal{R}_X > 1$ indicates improved sensitivity. When a static veto is used and the pseudorapidity range increased, the vetoing of jets outside the central region reduces background rates while simultaneously reducing the signal rates, thereby maintaining a similar signal-to-background efficiency as in the reference analysis. For the dynamic veto, however, there is a uniform $\mathcal{O}(5 - 20)\%$ improvement for most of the parameter space due to slightly higher background rejection coupled with a smaller decrease in signal efficiency. We anticipate this behavior to hold for all other dynamic veto schemes considered in this analysis.

Impact of Jet Vetoes When Lifting The M_{T2} Cut

As shown in Table 2, requiring the selection cut $M_{T2} > 90$ GeV greatly suppresses electroweak diboson and top quark pair production independently of a jet veto. However, the cut also reduces considerably the signal acceptance when sparticles are mass-degenerate. Notably, we report that choosing a more aggressive dynamic jet veto can control the top pair background sufficiently in the absence of the M_{T2} cut, leading to a significant improvement in sensitivity.

We have checked that using $H_T < p_T^{\prime 2}$ as a dynamic veto is stringent enough to control the top pair background when lifting the M_{T2} cut, independently of the signal region. When relaxing M_{T2} , total background rates grow by a factor of 5 for the lowest \cancel{E}_T signal region up to a factor of 1.5 for the highest \cancel{E}_T signal region, while there is a large, overall increase in signal efficiency. For the benchmark point $(m_{\tilde{\mu}_R}, m_{\tilde{\chi}_1}) = (750 \text{ GeV}, 700 \text{ GeV})$, this results in negligible changes in the signal (S) over background (B) ratio S/B for the two lower \cancel{E}_T signal regions but significant increases in S/B for the two higher \cancel{E}_T signal regions. Lifting the M_{T2} cut when using a stringent dynamic veto based on H_T therefore allows for improvements in sensitivity in the compressed region, independently of the integrated luminosity, due to the top pair background being sufficiently controlled by the dynamic veto itself.

We find though that the improvement does not hold for all veto schemes considered. When requiring $p_T^{\prime 1} < p_T^{\prime 2}$ and

no M_{T2} restriction, the top pair background comes to dominate the background rate in the two lower \cancel{E}_T signal regions and increases the rates by factors of 20 – 30, thereby reducing S/B , despite the increased signal efficiency. The two higher \cancel{E}_T signal regions are less affected due to a much smaller the top pair contribution, with only a factor of 2 increase in the total background rate for the highest \cancel{E}_T one. For $(m_{\tilde{\mu}_R}, m_{\tilde{\chi}_1}) = (750 \text{ GeV}, 700 \text{ GeV})$, we see a reduction in S/B in all signal regions, except for the highest \cancel{E}_T one, suggesting that the simplest incarnations of dynamic jet vetoes are not sufficient in their own right. This was noted previously in refs. [38, 39].

6 Summary and Conclusion

In summary, we have investigated several measures of leptonic and hadronic activities in the process

$$pp \rightarrow \gamma^*/Z^* + X \rightarrow \tilde{\mu}_R^+ \tilde{\mu}_R^- + X \rightarrow \mu^+ \mu^- + \cancel{E}_T + X, \quad (16)$$

and the associated SM background processes, to explore possible generalizations of dynamic jet vetoes. Using this information, we have demonstrated that a general class of dynamic jet vetoes can be used to improve the sensitivity of searches for right-handed smuon pair production at the LHC. The improvement becomes more significant as we probe mass scales further above the EW scales, and in some instances hold even when the final-state particles are soft. Most choices of measures for hadronic and leptonic activities perform better than the CMS-inspired benchmark analysis, which features a static jet veto threshold of $p_T^{\text{Veto}} = 25$ GeV (see fig. 5). Differences suggest that no single dynamic veto scheme will always be ideal but rather should be investigated on an analysis-by-analysis basis. Qualitatively, we find that dynamic jet vetoes using more inclusive measures of the hadronic activity, e.g., H_T , perform best, while the ideal choice of leptonic activity depends on the signal kinematics (see sec. 5). The impact of enlarging the jet veto rapidity window and complementarity to other selection cuts were also addressed.

Due to the dynamic nature of these cuts, sensitivity can likely be considerably improved with machine learning techniques and such future investigations are encouraged. Our results should generalize to other searches for new, heavy, uncolored physics that employ jet vetoes at the LHC. We push for further investigations in this direction.

Acknowledgements Kate Pachal and Fibonacci Tamarit are thanked for fruitful discussions over fondue and curry, respectively. This work has been partly supported by French state funds managed by the Agence Nationale de la Recherche (ANR) in the context of the LABEX ILP (ANR-11-IDEX-0004-02, ANR-10-LABX-63), which in particular funds the scholarship of SLW. KN is supported by the NWO. KN and SLW acknowledge the generous hospitality of CP3 at UCLouvain.

RR is supported under F.R.S.-FNRS under the ‘‘Excellence of Science’’ EOS be.h Project No 30820817, the MSCA co-fund ‘‘MOVE-IN Louvain,’’ and acknowledges the pleasant hospitality of the LPTHE.

References

1. H. P. Nilles, Phys. Rept. **110**, 1 (1984). doi:10.1016/0370-1573(84)90008-5
2. H. E. Haber and G. L. Kane, Phys. Rept. **117**, 75 (1985). doi:10.1016/0370-1573(85)90051-1
3. M. Aaboud *et al.* [ATLAS Collaboration], Phys. Rev. D **96**, no. 11, 112010 (2017) doi:10.1103/PhysRevD.96.112010 [arXiv:1708.08232 [hep-ex]].
4. M. Aaboud *et al.* [ATLAS Collaboration], Phys. Rev. D **97**, no. 11, 112001 (2018) doi:10.1103/PhysRevD.97.112001 [arXiv:1712.02332 [hep-ex]].
5. A. M. Sirunyan *et al.* [CMS Collaboration], Eur. Phys. J. C **77**, no. 10, 710 (2017) doi:10.1140/epjc/s10052-017-5267-x [arXiv:1705.04650 [hep-ex]].
6. A. M. Sirunyan *et al.* [CMS Collaboration], JHEP **1805**, 025 (2018) doi:10.1007/JHEP05(2018)025 [arXiv:1802.02110 [hep-ex]].
7. B. Fuks, M. Klasen, D. R. Lamprea and M. Rothering, JHEP **1210**, 081 (2012) doi:10.1007/JHEP10(2012)081 [arXiv:1207.2159 [hep-ph]].
8. B. Fuks, M. Klasen, D. R. Lamprea and M. Rothering, JHEP **1401**, 168 (2014) doi:10.1007/JHEP01(2014)168 [arXiv:1310.2621, arXiv:1310.2621 [hep-ph]].
9. A. M. Sirunyan *et al.* [CMS Collaboration], [arXiv:1806.05264 [hep-ex]].
10. M. Aaboud *et al.* [ATLAS Collaboration], Eur. Phys. J. C **78**, no. 12, 995 (2018) doi:10.1140/epjc/s10052-018-6423-7 [arXiv:1803.02762 [hep-ex]].
11. M. Aaboud *et al.* [ATLAS Collaboration], Phys. Rev. D **98**, no. 3, 032009 (2018) doi:10.1103/PhysRevD.98.032009 [arXiv:1804.03602 [hep-ex]].
12. M. Aaboud *et al.* [ATLAS Collaboration], Phys. Rev. D **98**, no. 9, 092012 (2018) doi:10.1103/PhysRevD.98.092012 [arXiv:1806.02293 [hep-ex]].
13. A. M. Sirunyan *et al.* [CMS Collaboration], JHEP **1803**, 160 (2018) doi:10.1007/JHEP03(2018)160 [arXiv:1801.03957 [hep-ex]].
14. P. Athron *et al.* [GAMBIT Collaboration], [arXiv:1809.02097 [hep-ph]].
15. V. D. Barger, K. m. Cheung, T. Han and R. J. N. Phillips, Phys. Rev. D **42**, 3052 (1990). doi:10.1103/PhysRevD.42.3052
16. V. D. Barger, K. m. Cheung, T. Han and D. Zeppenfeld, Phys. Rev. D **44**, 2701 (1991) Erratum: [Phys. Rev. D **48**, 5444 (1993)]. doi:10.1103/PhysRevD.48.5444, 10.1103/PhysRevD.44.2701
17. J. D. Bjorken, Phys. Rev. D **47**, 101 (1993). doi:10.1103/PhysRevD.47.101
18. R. S. Fletcher and T. Stelzer, Phys. Rev. D **48**, 5162 (1993) doi:10.1103/PhysRevD.48.5162 [hep-ph/9306253].
19. V. D. Barger, R. J. N. Phillips and D. Zeppenfeld, Phys. Lett. B **346**, 106 (1995) doi:10.1016/0370-2693(95)00008-9 [hep-ph/9412276].
20. A. Banfi, P. F. Monni, G. P. Salam and G. Zanderighi, Phys. Rev. Lett. **109**, 202001 (2012) doi:10.1103/PhysRevLett.109.202001 [arXiv:1206.4998 [hep-ph]].
21. T. Becher, M. Neubert and L. Rothen, JHEP **1310**, 125 (2013) doi:10.1007/JHEP10(2013)125 [arXiv:1307.0025 [hep-ph]].
22. I. W. Stewart, F. J. Tackmann, J. R. Walsh and S. Zuberi, Phys. Rev. D **89**, no. 5, 054001 (2014) doi:10.1103/PhysRevD.89.054001 [arXiv:1307.1808 [hep-ph]].
23. P. Meade, H. Ramani and M. Zeng, Phys. Rev. D **90**, no. 11, 114006 (2014) doi:10.1103/PhysRevD.90.114006 [arXiv:1407.4481 [hep-ph]].
24. P. Jaiswal and T. Okui, Phys. Rev. D **90**, no. 7, 073009 (2014) doi:10.1103/PhysRevD.90.073009 [arXiv:1407.4537 [hep-ph]].
25. P. F. Monni and G. Zanderighi, JHEP **1505**, 013 (2015) doi:10.1007/JHEP05(2015)013 [arXiv:1410.4745 [hep-ph]].
26. S. Gangal, M. Stahlhofen and F. J. Tackmann, Phys. Rev. D **91**, no. 5, 054023 (2015) doi:10.1103/PhysRevD.91.054023 [arXiv:1412.4792 [hep-ph]].
27. T. Becher, R. Frederix, M. Neubert and L. Rothen, Eur. Phys. J. C **75**, no. 4, 154 (2015) doi:10.1140/epjc/s10052-015-3368-y [arXiv:1412.8408 [hep-ph]].
28. S. Gangal, J. R. Gaunt, M. Stahlhofen and F. J. Tackmann, JHEP **1702**, 026 (2017) doi:10.1007/JHEP02(2017)026 [arXiv:1608.01999 [hep-ph]].
29. J. K. L. Michel, P. Pietrulewicz and F. J. Tackmann, [arXiv:1810.12911 [hep-ph]].
30. I. W. Stewart, F. J. Tackmann and W. J. Waalewijn, Phys. Rev. Lett. **106**, 032001 (2011) doi:10.1103/PhysRevLett.106.032001 [arXiv:1005.4060 [hep-ph]].
31. C. F. Berger, C. Marcantonini, I. W. Stewart, F. J. Tackmann and W. J. Waalewijn, JHEP **1104**, 092 (2011) doi:10.1007/JHEP04(2011)092 [arXiv:1012.4480 [hep-ph]].

32. T. Becher and M. Neubert, JHEP **1207**, 108 (2012) doi:10.1007/JHEP07(2012)108 [arXiv:1205.3806 [hep-ph]].
33. H. Baer, C. h. Chen, F. Paige and X. Tata, Phys. Rev. D **49**, 3283 (1994) doi:10.1103/PhysRevD.49.3283 [hep-ph/9311248].
34. H. Baer, C. h. Chen, F. Paige and X. Tata, Phys. Rev. D **53**, 6241 (1996) doi:10.1103/PhysRevD.53.6241 [hep-ph/9512383].
35. F. J. Tackmann, W. J. Waalewijn and L. Zeune, JHEP **1607**, 119 (2016) doi:10.1007/JHEP07(2016)119 [arXiv:1603.03052 [hep-ph]].
36. M. A. Ebert, S. Liebler, I. Moul, I. W. Stewart, F. J. Tackmann, K. Tackmann and L. Zeune, Phys. Rev. D **94**, no. 5, 051901 (2016) doi:10.1103/PhysRevD.94.051901 [arXiv:1605.06114 [hep-ph]].
37. B. Fuks and R. Ruiz, JHEP **1705**, 032 (2017) doi:10.1007/JHEP05(2017)032 [arXiv:1701.05263 [hep-ph]].
38. S. Pascoli, R. Ruiz and C. Weiland, Phys. Lett. B **786**, 106 (2018) doi:10.1016/j.physletb.2018.08.060 [arXiv:1805.09335 [hep-ph]].
39. S. Pascoli, R. Ruiz and C. Weiland, arXiv:1812.08750 [hep-ph].
40. D. Binosi and L. Theussl, Comput. Phys. Commun. **161**, 76 (2004) doi:10.1016/j.cpc.2004.05.001 [hep-ph/0309015].
41. M. J. Baker and A. Thamm, JHEP **1810**, 187 (2018) doi:10.1007/JHEP10(2018)187 [arXiv:1806.07896 [hep-ph]].
42. A. Alloul, N. D. Christensen, C. Degrande, C. Duhr and B. Fuks, Comput. Phys. Commun. **185**, 2250 (2014) doi:10.1016/j.cpc.2014.04.012 [arXiv:1310.1921 [hep-ph]].
43. C. Degrande, Comput. Phys. Commun. **197**, 239 (2015) doi:10.1016/j.cpc.2015.08.015 [arXiv:1406.3030 [hep-ph]].
44. T. Hahn, Comput. Phys. Commun. **140**, 418 (2001) doi:10.1016/S0010-4655(01)00290-9 [hep-ph/0012260].
45. C. Degrande, C. Duhr, B. Fuks, D. Grellscheid, O. Mattelaer and T. Reiter, Comput. Phys. Commun. **183**, 1201 (2012) doi:10.1016/j.cpc.2012.01.022 [arXiv:1108.2040 [hep-ph]].
46. J. Alwall *et al.*, JHEP **1407**, 079 (2014) doi:10.1007/JHEP07(2014)079 [arXiv:1405.0301 [hep-ph]].
47. S. Frixione and B. R. Webber, JHEP **0206**, 029 (2002) doi:10.1088/1126-6708/2002/06/029 [hep-ph/0204244].
48. P. Artoisenet, R. Frederix, O. Mattelaer and R. Rietkerk, JHEP **1303**, 015 (2013) doi:10.1007/JHEP03(2013)015 [arXiv:1212.3460 [hep-ph]].
49. J. Alwall, C. Duhr, B. Fuks, O. Mattelaer, D. G. ÅÛztÅijrk and C. H. Shen, Comput. Phys. Commun. **197**, 312 (2015) doi:10.1016/j.cpc.2015.08.031 [arXiv:1402.1178 [hep-ph]].
50. T. SjÅÛstrand *et al.*, Comput. Phys. Commun. **191**, 159 (2015) doi:10.1016/j.cpc.2015.01.024 [arXiv:1410.3012 [hep-ph]].
51. P. Skands, S. Carrazza and J. Rojo, Eur. Phys. J. C **74**, no. 8, 3024 (2014) doi:10.1140/epjc/s10052-014-3024-y [arXiv:1404.5630 [hep-ph]].
52. E. Conte, B. Fuks and G. Serret, Comput. Phys. Commun. **184**, 222 (2013) doi:10.1016/j.cpc.2012.09.009 [arXiv:1206.1599 [hep-ph]].
53. E. Conte and B. Fuks, Int. J. Mod. Phys. A **33**, no. 28, 1830027 (2018) doi:10.1142/S0217751X18300272 [arXiv:1808.00480 [hep-ph]].
54. M. Cacciari, G. P. Salam and G. Soyez, JHEP **0804**, 063 (2008) doi:10.1088/1126-6708/2008/04/063 [arXiv:0802.1189 [hep-ph]].
55. M. Cacciari, G. P. Salam and G. Soyez, Eur. Phys. J. C **72**, 1896 (2012) doi:10.1140/epjc/s10052-012-1896-2 [arXiv:1111.6097 [hep-ph]].
56. V. Bertone *et al.* [NNPDF Collaboration], SciPost Phys. **5**, no. 1, 008 (2018) doi:10.21468/SciPostPhys.5.1.008 [arXiv:1712.07053 [hep-ph]].
57. A. Buckley, J. Ferrando, S. Lloyd, K. NordstrÅÛm, B. Page, M. RÅijfenacht, M. SchÅÛnherr and G. Watt, Eur. Phys. J. C **75**, 132 (2015) doi:10.1140/epjc/s10052-015-3318-8 [arXiv:1412.7420 [hep-ph]].
58. B. Fuks, M. Klasen, D. R. Lamprea and M. Rothering, Eur. Phys. J. C **73**, 2480 (2013) doi:10.1140/epjc/s10052-013-2480-0 [arXiv:1304.0790 [hep-ph]].
59. M. Bonvini *et al.*, JHEP **1509**, 191 (2015) doi:10.1007/JHEP09(2015)191 [arXiv:1507.01006 [hep-ph]].
60. J. Fiaschi and M. Klasen, JHEP **1803**, 094 (2018) doi:10.1007/JHEP03(2018)094 [arXiv:1801.10357 [hep-ph]].
61. J. F. Guion, M. Herrero and A. Mendez, Phys. Rev. D **37**, 2533 (1988). doi:10.1103/PhysRevD.37.2533
62. G.-C. Cho, K. Hagiwara, J. Kanzaki, T. Plehn, D. Rainwater and T. Stelzer, Phys. Rev. D **73**, 054002 (2006) doi:10.1103/PhysRevD.73.054002 [hep-ph/0601063].
63. P. Konar and D. Zeppenfeld, Phys. Lett. B **647**, 460 (2007) doi:10.1016/j.physletb.2007.02.037 [hep-ph/0612119].
64. F. Borzumati and K. Hagiwara, JHEP **1103**, 103 (2011) doi:10.1007/JHEP03(2011)103 [arXiv:0912.0454 [hep-ph]].
65. J. M. Lindert, F. D. Steffen and M. K. Trenkel, JHEP **1108**, 151 (2011) doi:10.1007/JHEP08(2011)151

- [arXiv:1106.4005 [hep-ph]].
66. M. Dasgupta, F. Dreyer, G. P. Salam and G. Soyez, *JHEP* **1504**, 039 (2015) doi:10.1007/JHEP04(2015)039 [arXiv:1411.5182 [hep-ph]].
67. A. Banfi, F. Caola, F. A. Dreyer, P. F. Monni, G. P. Salam, G. Zanderighi and F. Dulat, *JHEP* **1604**, 049 (2016) doi:10.1007/JHEP04(2016)049 [arXiv:1511.02886 [hep-ph]].
68. M. Dasgupta, F. A. Dreyer, G. P. Salam and G. Soyez, *JHEP* **1606**, 057 (2016) doi:10.1007/JHEP06(2016)057 [arXiv:1602.01110 [hep-ph]].
69. M. Dasgupta, L. Magnea and G. P. Salam, *JHEP* **0802**, 055 (2008) doi:10.1088/1126-6708/2008/02/055 [arXiv:0712.3014 [hep-ph]].
70. T. Aaltonen *et al.* [CDF Collaboration], *Phys. Rev. Lett.* **101**, 251801 (2008) doi:10.1103/PhysRevLett.101.251801 [arXiv:0808.2446 [hep-ex]].
71. G. Aad *et al.* [ATLAS Collaboration], *Phys. Lett. B* **718**, 879 (2013) doi:10.1016/j.physletb.2012.11.058 [arXiv:1208.2884 [hep-ex]].
72. G. Aad *et al.* [ATLAS Collaboration], *JHEP* **1405**, 071 (2014) doi:10.1007/JHEP05(2014)071 [arXiv:1403.5294 [hep-ex]].
73. V. Khachatryan *et al.* [CMS Collaboration], *Eur. Phys. J. C* **74**, no. 9, 3036 (2014) doi:10.1140/epjc/s10052-014-3036-7 [arXiv:1405.7570 [hep-ex]].
74. G. Aad *et al.* [ATLAS Collaboration], *JHEP* **1410**, 096 (2014) doi:10.1007/JHEP10(2014)096 [arXiv:1407.0350 [hep-ex]].
75. G. Aad *et al.* [ATLAS Collaboration], *Phys. Rev. D* **93**, no. 5, 052002 (2016) doi:10.1103/PhysRevD.93.052002 [arXiv:1509.07152 [hep-ex]].
76. A. M. Sirunyan *et al.* [CMS Collaboration], *JHEP* **1803**, 166 (2018) doi:10.1007/JHEP03(2018)166 [arXiv:1709.05406 [hep-ex]].
77. K. O. Mikaelian, *Phys. Rev. D* **17**, 750 (1978), doi:10.1103/PhysRevD.17.750
78. R. W. Brown, D. Sahdev and K. O. Mikaelian, *Phys. Rev. D* **20**, 1164 (1979), doi:10.1103/PhysRevD.20.1164
79. K. O. Mikaelian, M. A. Samuel and D. Sahdev, *Phys. Rev. Lett.* **43**, 746 (1979), doi:10.1103/PhysRevLett.43.746
80. D. p. Zhu, *Phys. Rev. D* **22**, 2266 (1980), doi:10.1103/PhysRevD.22.2266
81. S. J. Brodsky and R. W. Brown, *Phys. Rev. Lett.* **49**, 966 (1982), doi:10.1103/PhysRevLett.49.966
82. R. W. Brown, K. L. Kowalski and S. J. Brodsky, *Phys. Rev. D* **28**, 624 (1983) Addendum: [*Phys. Rev. D* **29**, 2100 (1984)]. doi:10.1103/PhysRevD.28.624, 10.1103/PhysRevD.29.2100
83. U. Baur, T. Han and J. Ohnemus, *Phys. Rev. D* **53**, 1098 (1996) doi:10.1103/PhysRevD.53.1098 [hep-ph/9507336].
84. T. Gehrmann, M. Grazzini, S. Kallweit, P. Maierh uffer, A. von Manteuffel, S. Pozzorini, D. Rathlev and L. Tancredi, *Phys. Rev. Lett.* **113**, no. 21, 212001 (2014) doi:10.1103/PhysRevLett.113.212001 [arXiv:1408.5243 [hep-ph]].
85. A. M. Sirunyan *et al.* [CMS Collaboration], *JHEP* **1809**, 065 (2018) doi:10.1007/JHEP09(2018)065 [arXiv:1805.05784 [hep-ex]].
86. *** Not Found with lookup: 'find r CMS-DP-2018-009'
87. CMS Collaboration [CMS Collaboration], CMS-PAS-EXO-15-006.
88. A. M. Sirunyan *et al.* [CMS Collaboration], *JINST* **12**, no. 10, P10003 (2017) doi:10.1088/1748-0221/12/10/P10003 [arXiv:1706.04965 [physics.ins-det]].
89. S. Chatrchyan *et al.* [CMS Collaboration], *JINST* **6**, P11002 (2011) doi:10.1088/1748-0221/6/11/P11002 [arXiv:1107.4277 [physics.ins-det]].
90. M. Aaboud *et al.* [ATLAS Collaboration], [arXiv:1807.09477 [hep-ex]].
91. C. G. Lester and D. J. Summers, *Phys. Lett. B* **463**, 99 (1999) doi:10.1016/S0370-2693(99)00945-4 [hep-ph/9906349].
92. H. C. Cheng and Z. Han, *JHEP* **0812**, 063 (2008) doi:10.1088/1126-6708/2008/12/063 [arXiv:0810.5178 [hep-ph]].
93. A. L. Read, *J. Phys. G* **28**, 2693 (2002), doi:10.1088/0954-3899/28/10/313
94. M. Aaboud *et al.* [ATLAS Collaboration], *Phys. Rev. D* **98**, 052005 (2018) doi:10.1103/PhysRevD.98.052005 [arXiv:1802.04146 [hep-ex]].